

Patterning of martensitic nanotwins

Yuan Zhong and Ting Zhu*

Woodruff School of Mechanical Engineering, Georgia Institute of Technology, Atlanta, GA 30332, USA

Received 21 July 2012; accepted 11 August 2012

Available online 19 August 2012

We perform the atomistic Monte Carlo simulations of formation of nanostructured martensites in nickel–titanium thin films. The results reveal the atomistically resolved patterning of martensitic nanotwins, including coarsening, branching and twinning within twins, as mediated by temperature and substrate constraints. A scaling law is derived to elucidate the physical effects governing the characteristic nanostructure length scale of the twin width. Our modeling approach opens up possibilities for the atomistically based design of martensitic nanostructures to produce advanced alloys with optimized properties.

© 2012 Acta Materialia Inc. Published by Elsevier Ltd. All rights reserved.

Keywords: Atomistic modeling; Martensite; Nanotwin; Monte Carlo simulation; Shape memory alloys

Advanced materials, such as shape memory alloys [1], ferroelectrics [2] and other multiferroics [3], are being increasingly used for a variety of multifunctional applications. In these materials, the formation of martensitic microstructures is commonly observed [4,5]. Understanding the physics and design principles of nanostructured martensite is crucial for the control of its properties, e.g. producing large reversible strains in response to thermomechanical stimuli in shape memory alloys.

Various theoretical and modeling approaches have been applied to study martensitic microstructures, including crystallographic and geometrically nonlinear theory [1,6], phase-field simulation [7,8], atomistic molecular dynamics [9,10] and quantum mechanical calculation [11,12]. While those studies have greatly advanced our understanding of nanostructured martensites [4,5], they often require a priori assumptions on the transformation geometry and energy function, or are limited in their spatial–temporal resolution. Here, we report a novel way to atomistically model martensitic nanostructures by combining the interatomic potential and the Monte Carlo (MC) method. Without geometrical construction and timescale limitations, our MC simulations reveal the atomistically resolved patterning of nanotwins in a model system of nickel–titanium (NiTi) thin film. The results provide insights into the length scale and temperature effects on the formation of martensitic nanostructures.

A Finnis–Sinclair [13] type many-body interatomic potential is employed to describe the NiTi system. Compared to quantum mechanical modeling, it enables atomic-level simulations in a much larger system, which is essential for the study of martensitic nanostructures. This potential was developed by Lai and Liu [14], and later improved to smooth the discontinuities at its cutoff [9]. To overcome the timescale limitation of molecular dynamics, we perform canonical Monte Carlo simulations (with the Metropolis algorithm [15]) to study the temperature-driven formation of twinned microstructures. We construct a NiTi thin film in the austenitic B2 phase. The system is 5.1 nm × 4.8 nm in the film plane and 16.8 nm thick, and involves a total of 23,040 atoms. Periodic boundary conditions are applied along both the $\langle 001 \rangle_{B2}$ and $\langle 1\bar{1}0 \rangle_{B2}$ directions within the film plane. The top surface is free to move in the vertical $\langle 110 \rangle_{B2}$ direction. Four bottom layers are fixed to the parent B2 phase, mimicking the constraint of the austenitic substrate.

The martensitic phase transformation starting temperature (M_s) in this NiTi thin film model system has been benchmarked to be around 260 K, lower than the bulk value of M_s (~ 310 K) predicted from our previous simulations [9]. This difference can be attributed to the boundary effects. Specifically, the atomic bonding environment at the free surface and fixed bottom is different from that in the bulk of the thin film, leading to a shift in the phase transformation temperature.

We perform the MC simulations in an NVT ensemble at various undercooling temperatures. For each

* Corresponding author; e-mail: ting.zhu@me.gatech.edu

temperature, tens of simulations are conducted to identify the possibly different metastable microstructures. Each of MC simulations involves 1.4 billion steps, ensuring the converged twin structure and energy. We present here the representative MC results at 250 K (~ 10 K undercooling) and 200 K (~ 60 K undercooling). Simulations at temperatures lower than 200 K yield results similar to those at 200 K.

Our MC simulations reveal the temperature-driven diffusionless phase transformation from the parent B2 to the martensitic B19 phase in the NiTi thin film at both 250 and 200 K. Figure 1(a) shows the schematic of the displacive B2 \rightarrow B19 transformation in a conventional unit cell. In the parent B2 phase, the cell edge is $\sqrt{2}a_0$ in both the $\langle 110 \rangle_{B2}$ and $\langle 1\bar{1}0 \rangle_{B2}$ directions, where a_0 denotes the B2 lattice constant. Upon phase transformation, the B19 phase forms two equivalent variants in the plane of the paper, with $c > \sqrt{2}a_0 > a$; the cell edge in the $\langle 001 \rangle_{B2}$ direction remains unchanged due to geometrical constraint of the austenitic substrate. Note that the previous molecular dynamics simulations with the same interatomic potential predicted the B2 \rightarrow B19' phase transformation in both NiTi bulk (temperature-driven) [9,10] and in a nanopillar (stress-driven) [16]. The favorable formation of the martensitic B19 phase in the thin film can be attributed to the small film thickness, resulting in an increasing role of the free surface and the fixed austenitic substrate in selecting the transformation product. Interestingly, the resultant martensitic B19 phase exhibits multiple variants, the periodic arrangement of which leads to nanotwin patterning.

Figure 1(b–d) shows the sequential process of nanotwin patterning at 250 K (~ 10 K lower than M_s). In Figure 1(b), the initiation of the B2 \rightarrow B19 transformation appears to be a homogeneous nucleation process. The atomic configuration on the left shows that the martensitic

itic B19 phase emerges as equally spaced circular nuclei, each of which involves a group of light blue atoms with a diameter about 1.5 nm. In the corresponding contour of lattice ratios on the right, it is seen that the nuclei with the same B19 variant (i.e. same color) are neighbored in the 45° direction. Those nuclei grow and coalesce to form the inclined twin stripes. Figure 1(c) shows an intermediate state, and Figure 1(d) the final converged structure of twinned martensite. Note that the above sequence represents a transformation path from an initial state to the mode of the stationary distribution along the Markov chain, and does not necessarily reflect the temporal evolution of martensitic phase transformation. A number of repeated MC simulations at 250 K all yield the same final product.

Both the atomic configuration and the contour of lattice ratios in Figure 1(d) reveal the periodic stripes of nanotwins, featuring an atomically sharp twin interface with its normal in the $\langle 100 \rangle_{B2}$ direction. Of particular note are the different twin widths in the periodic nanotwinned stripes, i.e. ~ 1.5 nm for variant I (red stripe) and ~ 2.0 nm for variant II (blue stripe). Correspondingly, the volume fraction of variant I, denoted as λ , is 0.42. This volume fraction can be readily rationalized on the basis of requirement of geometrical compatibility at the habit plane between the martensitic twins and austenitic substrate [1], i.e. $\lambda\alpha + (1 - \lambda)\gamma = 1$, where $\gamma = c/(\sqrt{2}a_0)$ and $\alpha = a/(\sqrt{2}a_0)$.

It should be emphasized that nanotwins near the substrate are not in their equilibrium states, as evidenced by the blurred von Mises shear strain plot and color map in Figure 1(d). This so-called transformation decay region results from the accommodation of lattice mismatch between the austenitic substrate and the twinned martensite. Such a decay region plays a key role in selecting the size of the nanotwin stripes. That is, the nanotwin width

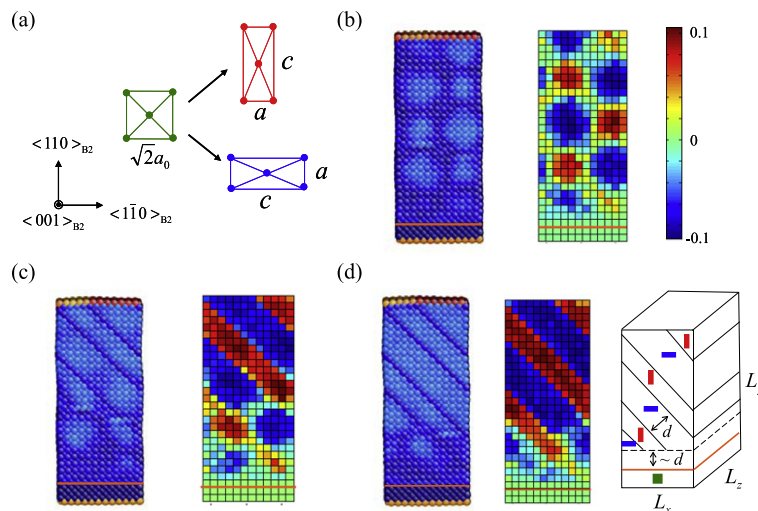


Figure 1. Martensitic transformation and nanotwin patterning in an NiTi thin film at 250 K (~ 10 K undercooling). The region below the red line is fixed to represent the austenitic substrate. (a) Schematic of the B2 to B19 transformation in a conventional unit cell. The unit cell deformation is exaggerated to increase the geometric contrast between the two B19 variants. (b) MC snapshot showing the initiation of martensitic phase transformation. (c) An intermediate state of formation of twinned martensite. (d) The final converged state with the fully developed periodic twin stripes. In (b–d), the left image shows the atomic configuration, where atoms are colored by the von Mises shear strain invariant, and the right one shows the contour of the ratio of the lattice constant in the $\langle 110 \rangle_{B2}$ direction over that in the $\langle 1\bar{1}0 \rangle_{B2}$ direction. In the schematic of twin stripes in (d), the two B19 variants are represented by the red and blue rectangle, respectively, and the B2 phase is represented by the green square. (For interpretation of the references to colour in this figure legend, the reader is referred to the web version of this article.)

is governed by the competition between the strain energy in the decay region and the twin interface energy in the film. Incidentally, a similar energy competition leads to periodic stripes in the strained liquid crystal elastomer, and a scaling analysis of stripe width has been given by Verwey and co-workers [17]. Along the same line of reasoning, we note that the size of the decay region is proportional to the twin width d , since the lattice distortion from the equilibrium B19 state (being either of the two B19 variants) is periodic in the L_x direction with a period of the order of d , as indicated in Figure 1(d). Hence the strain energy per stripe is $\sim \mu \epsilon^2 d^2 L_z$, where μ is the shear modulus and ϵ is the characteristic lattice strain in the stripe. There are L_x/d stripes in the film. As a result, the total elastic energy in the decay region is $\sim \mu \epsilon^2 L_x L_z d$. On the other hand, the total interfacial energy associated with twin boundaries is $\sim f_{\text{TB}} L_x L_y L_z / d$, where f_{TB} is the twin boundary energy per unit area. Minimization of the sum of the above elastic and interfacial energies with respect to d yields the optimal twin width

$$d \sim \sqrt{\frac{f_{\text{TB}} L_y}{\mu \epsilon^2 L_x}} \quad (1)$$

The scaling relation of Eq. (1) elucidates the physical factors governing the characteristic twin width. It depends on the geometric mean of two length scales: one is the extrinsic sample length scale of the film thickness L_y and the other is the intrinsic material length scale of $\xi \equiv f_{\text{TB}} / (\mu \epsilon^2)$ that scales with the twin boundary thickness [17]. Using the typical values of NiTi martensite [9], $f_{\text{TB}} \sim 0.1 \text{ J/m}^2$, $\mu \sim 50 \text{ GPa}$ and $\epsilon \sim 0.05$, we estimate $\xi \sim 1 \text{ nm}$. Given that $L_y = 16.8 \text{ nm}$ in our MC simulations, Eq. (1) predicts the twin width d to be in the range of a few nanometers, consistent with our MC results. Moreover, since μ increases with decreasing temperature and usually has a stronger temperature dependence than f_{TB} [17], Eq. (1) suggests that an increase in undercooling can lead to twin refinement. This has been verified by our MC simulations, to be detailed next.

Large undercooling can yield a variety of patterning in nanotwinned martensite. Figure 2(a) shows the converged martensitic microstructure at 200 K. The nanotwinned stripes consist of alternating B19 variants similar to those at 250 K, as shown in Figure 1(d). However, the twin width decreases, as does the size of the transformation decay region. This twin refinement with decreasing temperature (equivalently, twin coarsening with increasing temperature) is consistent with the prediction from our previous scaling analysis.

More interestingly, repeated MC simulations reveal the branching of nanotwins near the habit plane between the martensitic twins and austenitic substrate. One scenario of twin branching is shown in Figure 2(b), where the coarse twins appear near the free surface and fine twins, aligned in the same orientation, occur when approaching the habit plane. Alternatively, the fine twins could form with twin boundaries in another equivalent $\{100\}_{\text{B2}}$ plane, as shown in Figure 2(c3). This produces an intriguing pattern of “twins within twins” [4], with the primary twin interface of $\{110\}_{\text{B2}}$ and the secondary twin interfaces of $\{100\}_{\text{B2}}$.

The branched nanotwins in Figure 2(b and c) are likely more favorable energetically than the non-branched ones in Figure 2(a). Along the lines of previous analysis of the energy competition in twinned martensite, it is understandable that the energy budget could be effectively reduced by adopting multiple twin sizes, e.g. coarse and fine twins coexist but are located at different places, as shown in our MC simulations. The fine twins near the habit plane lower the elastic energy by reducing the size of the decay region. On the other hand, the coarse twins near the free surface reduce the overall twin interfacial energy.

Figure 2(c1–c3) shows the sequential process of nucleation and growth of the branched nanotwins, with their converged state shown in Figure 2(c3). In contrast to the homogeneous nucleation of martensite within the bulk of the thin film at 250 K in Figure 1(b), the martensitic nanotwins nucleate simultaneously near the free surface and the substrate at 200 K. They exhibit differ-

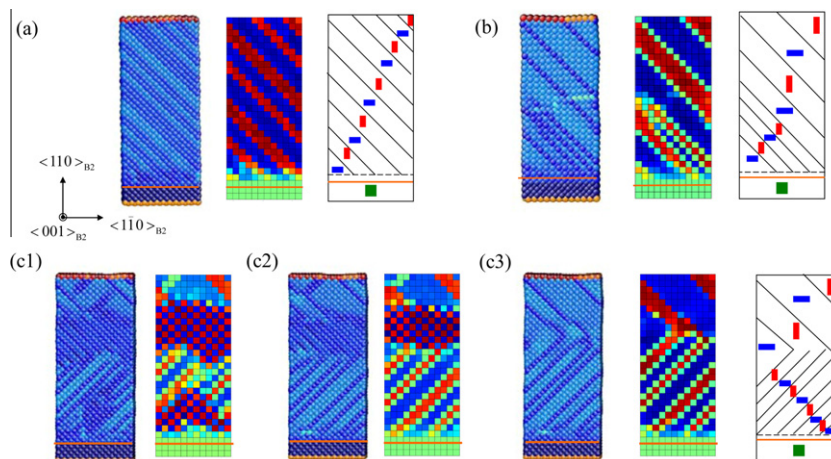


Figure 2. Refinement and branching of nanotwins at 200 K ($\sim 60 \text{ K}$ undercooling). (a) The final converged state from a MC simulation showing the refined twin stripes, as opposed to the coarse ones in Figure 1(d). (b) Branched nanotwins with twin boundaries aligned in the same orientation. (c) Sequential process of formation of branched nanotwins; in contrast to (b), the branched twin boundaries form in another, equivalent $\{100\}_{\text{B2}}$ plane. The color scheme in (a–c) is the same as in Figure 1. (For interpretation of the references to colour in this figure legend, the reader is referred to the web version of this article.)

ent twin widths and grow to meet inside the thin film, yielding the final product shown in Figure 2(c3). The geometrical constraints near the free surface and the habit plane are distinctly different, setting the different characteristic twin sizes. The apparent branching of nanotwins actually results from the simultaneous nucleation of nanotwins from both the free surface and the habit plane. Different branching modes in Figure 2(b and c) originate from the random orientation of nanotwins when they are initiated.

In summary, we develop an atomistic Monte Carlo method to simulate the formation of martensitic nanostructures without timescale limitations. The results demonstrate the temperature-mediated patterning of nanotwins in alloy thin films. This modeling approach can be applied to the atomistically based design of martensitic nanostructures to produce advanced alloys with optimized properties.

Support by the NSF Grant CMMI-0825435 is greatly acknowledged.

- [1] K. Otsuka, X. Ren, *Prog. Mater. Sci.* 50 (2005) 511.
- [2] D.G. Schlom, L.Q. Chen, C.B. Eom, K.M. Rabe, S.K. Streiffer, J.M. Triscone, *Annu. Rev. Mater. Res.* 37 (2007) 589.
- [3] A. Saxena, G. Aeppli, *MRS Bull.* 34 (2009) 804.
- [4] S. Kaufmann, R. Niemann, T. Thersleff, U.K. Rossler, O. Heczko, J. Buschbeck, B. Holzapfel, L. Schultz, S. Fahler, *New J. Phys.* 13 (2011) 053029.
- [5] T. Zhu, J. Li, *Prog. Mater. Sci.* 55 (2010) 710.
- [6] K. Bhattacharya, *Microstructure of Martensite. Why it Forms and How it Gives Rise to the Shape-Memory Effect*, Oxford University Press, Oxford, 2003.
- [7] L.Q. Chen, *Annu. Rev. Mater. Res.* 32 (2002) 113.
- [8] Y.C. Shu, J.H. Yen, *Acta Mater.* 56 (2008) 3969.
- [9] Y. Zhong, K. Gall, T. Zhu, *J. Appl. Phys.* 110 (2011) 033532.
- [10] D. Mütter, P. Nielaba, *Phys. Rev. B* 82 (2010) 224201.
- [11] T. Waitz, D. Spisak, J. Hafner, H.P. Karnthaler, *Europhys. Lett.* 71 (2005) 98.
- [12] N. Hatcher, O.Y. Kontsevoi, A.J. Freeman, *Phys. Rev. B* 79 (2009) 020202.
- [13] M.W. Finnis, J.E. Sinclair, *Philos. Mag. A* 50 (1984) 45.
- [14] W.S. Lai, B.X. Liu, *J. Phys.: Condens. Matter* 12 (2000) L53.
- [15] N. Metropolis, A.W. Rosenbluth, M.N. Rosenbluth, A.H. Teller, E. Teller, *J. Chem. Phys.* 21 (1953) 1087.
- [16] Y. Zhong, K. Gall, T. Zhu, *Acta Mater.* (2012), <http://dx.doi.org/10.1016/j.actamat.2012.08.004>.
- [17] G.C. Verwey, M. Warner, E.M. Terentjev, *J. Phys. II* (6) (1996) 1273.